Comparative Response Assessment of Minimally Compliant Low-Rise Base-Isolated and Conventional Steel Moment-Resisting Frame Buildings

Prayag J. Sayani[1]; Emrah Erduran[2]; and Keri L. Ryan, M.ASCE[3]

Abstract: In this study, the multihazard response of code-designed conventional and base-isolated steel frame buildings is evaluated using nonlinear response history analysis. The results of hazard and structural response analysis for 3-story moment-resisting frame buildings are presented in this paper. Three-dimensional models for both buildings are created, and seismic response is assessed for three scenario earthquakes. The response history analysis results indicate that the performance of the isolated building is superior to the conventional building in the design event. However, for the Maximum Considered Earthquake, the presence of outliers in the response data reduces confidence that the isolated building provides superior performance to its conventional counterpart. The potential causes of the outliers have been carefully evaluated. **DOI: 10.1061/(ASCE)ST.1943-541X.0000358.**

CE Database subject headings: Acceleration; Base isolation; Ductility; Nonlinear analysis; Performance characteristics; Response spectra; Seismic effects; Structural response; Low-rise buildings; Frames.

Author keywords: Acceleration; Base isolation; Ductility; Nonlinear analysis; Performance characteristics; Response spectra; Seismic effects; Structural response.

Introduction

The principal benefit of seismic isolation for buildings—to offer far superior performance in a design level earthquake—is generally accepted and recognized by structural engineers. With seismic isolation, flexible devices installed at the base lengthen or shift the building's natural period to the low acceleration region of the spectrum. Consequently, an isolated building accommodates the lower design forces elastically, and structural damage is eliminated or greatly reduced relative to a conventional building that accommodates the design forces through inelastic response. Furthermore, nonstructural components and building contents, which make up at least 80% of the building's value [Applied Technology Council (ATC) 2008; Taghavi and Miranda 2003], are also better protected in an isolated building because of lowered acceleration demands.

In the United States, seismic performance objectives, which differ for isolated and conventional systems, are only implicitly embedded in code design standards [ASCE 2005; International Code Council (ICC) 2006, Building Seismic Safety Council (BSSC) 2004]. These codes provide design standards with reference to a single earthquake intensity level, a design earthquake with a 10% probability of occurring in a 50-year window. The code objective for this event is to limit damage in a conventional building through controlled yielding of ductile components, such that life safety is preserved. In an isolated building, the objective is to prevent damage of structural components through elastic response and prevent damage of nonstructural components through reduced accelerations. Although it is expected that the performance objectives for an isolated building are met, the vast majority of isolated buildings are designed beyond minimum code compliance because of owner objectives or jurisdiction requirements, which compounds costs and leads to the impression that seismic isolation is too expensive for typical projects.

Emerging techniques, such as those used for economic analysis and life cycle performance assessment (ATC 2009a), will require multilevel response evaluation. The intuitive assumption that superior performance of an isolated building in a design event naturally leads to superior performance in other earthquake scenarios deserves critical examination. Yielding of the isolated superstructure in extreme events is likely, and the associated response trends have been examined by many (Pinto and Vanzi 1992; Palazzo and Petti 1996; Ceccoli et al. 1999; Naaseh et al. 2002; Ordonez et al. 2003; Politopoulos and Sollogoub 2005; Kikuchi et al. 2008; Sayani and Ryan 2009). A key observation is that an isolated structure, on yielding, accumulates ductility demands in the superstructure more quickly than a comparable conventional building, and thus the drift demand in the isolated superstructure can in fact be greater than in a comparable conventional building. FEMA P695 (ATC 2009b) concluded that, when designed by current code standards, conventional and seismic isolated RC buildings have about the same probability

[1]Structural Engineer, Gandhi Engineering, Inc., 111 John St., 3rd Floor, New York, NY 10038; formerly, Ph.D. Candidate, Dept. of Civil and Environmental Engineering, Utah State Univ., Logan, UT 84322-4110.

[2]Research Engineer, NORSAR, Gunnar Randers vei 15, P.O. Box 53, NO-2027, Kjeller, Norway; formerly, Post-Doctorate Researcher, Dept. of Civil and Environmental Engineering, Utah State Univ., Logan, UT 84322-4110.

[3]Assistant Professor, Dept. of Civil and Environmental Engineering, Univ. of Nevada, Reno/MS 0258, Reno, NV 89557-0258; formerly, Assistant Prof., Dept. of Civil and Environmental Engineering, Utah State Univ., Logan, UT 84322-4110 (corresponding author). E-mail: keri.ryan@unr.edu

Note. This manuscript was submitted on July 7, 2009; approved on December 15, 2010; published online on December 17, 2010. Discussion period open until March 1, 2012; separate discussions must be submitted for individual papers. This paper is part of the ***Journal of Structural Engineering***, Vol. 137, No. 10, October 1, 2011. ©ASCE, ISSN 0733-9445/2011/10-1118–1131/$25.00.

of collapse in the Maximum Considered Earthquake (MCE). Furthermore, response of an isolated building attributable to a "frequent" earthquake intensity may be suboptimal when large isolator deformations are anticipated in the design event.

A number of studies have performed comparative response evaluation of isolated and conventional buildings (e.g., Shenton and Lin 1993; Lin and Shenton 1992; Hall and Ryan 2000; Dolce and Cardone 2003; Hamidi et al. 2003; Agarwal et al. 2007; Dolce et al. 2007). Some have evaluated the buildings in reference to code standards. Researchers (Lin and Shenton 1992; Shenton and Lin 1993) compared the response of concrete and steel frames designed to the 1991 Uniform Building Code. However, the seismic provisions of building codes have evolved rapidly over the years, and to the best of the authors' knowledge, a comparative evaluation of code-designed buildings using ground motions systematically selected to represent multiple hazards has not been performed.

The objective of this study is to comparatively evaluate the multilevel seismic response of minimally code-compliant 3-story conventional and base-isolated steel moment-resisting frame buildings. A moment frame has been selected to address whether a similar benefit can be provided by applying isolation to a relatively flexible lateral system compared with an ideal stiff system. Post-Northridge moment-resisting frames are attractive, providing reliable seismic performance and allowing for flexibility of architectural design. A number of midrise steel moment frame isolated buildings are in various phases of the design and construction process in California. Ground motions are selected for three distinct earthquake scenarios representing 2, 10, and 50% probabilities of exceedance in 50 years. Statistical responses determined from nonlinear response history analysis of high fidelity three-dimensional numerical simulation models are presented and analyzed.

Design and Modeling Assumptions for the Buildings

Design Assumptions

Hypothetical 3-story conventional and base-isolated moment-resisting frame buildings were designed by Forell/Elsesser Engineers Inc. for use in this study. These office buildings (occupancy category II and importance factor $I = 1.0$) were designed by the Equivalent Lateral Force Method to meet the requirements of 2006 International Building Code (ICC 2006), ASCE 7-05 (ASCE 2005), and AISC 341-05 (AISC 2005). The buildings were designed for a Los Angeles, California, location (34.50 N, 118.2 W) on stiff soil (site class D with reference shear wave velocity of 180 to 360 m/s). The mapped spectral accelerations for this location are $S_s = 2.2$ g for short periods and $S_1 = 0.74$ g for a 1-s period (g = gravitational acceleration).

The conventional building was detailed for high ductility as a special moment-resisting frame (SMRF) and uses reduced beam section (RBS) connections, which are prequalified according to AISC 341-05 (AISC 2005). However, the isolated building, which has lower ductility requirements, was detailed as an intermediate moment-resisting frame (IMRF) utilizing welded unreinforced flange, welded web (WUF-W) beam-column connections. As such, design force reduction factors were $R = 8$ for the SMRF, and $R_I = 1.67$ for the isolated IMRF—assuming a design yield strength of 345 MPa (50 ksi) for structural steel. Design drift limits were 2.5% for the SMRF and 1.5% for the isolated IMRF, and the design of both buildings was drift controlled.

The building configurations are based on the plan layout for the 3-story buildings designed for the SAC Steel Project (FEMA 2000a) with modifications (Fig. 1). The buildings are 55 by 36.6 m (180 by 120 ft) in plan, with story heights of 4.57 m (15 ft) and column spacing of 9.15 m (30 ft) in each direction. Lateral resistance is provided by two 5-bay perimeter moment frames in the X-direction and two 3-bay perimeter and two 2-bay interior moment frames in the Y-direction; moment-resisting bays are indicated by bold lines in Fig. 1. The steel sections selected for the moment-resisting frame members are listed in Table 1.

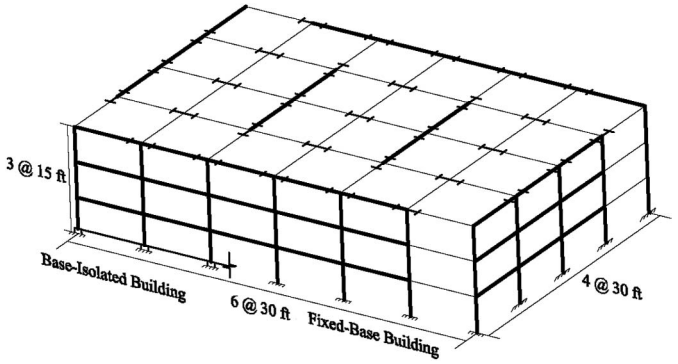

Fig. 1. 3D view of the building elevation and plan layout

Table 1. Member Sizes for the Conventional SMRF and Isolated IMRF

Frame	Story	Columns	Beams
SMRF	Roof	W14 × 211	W27 × 102
	2	W14 × 370	W33 × 130
	1	W14 × 370	W33 × 141
IMRF	Roof	W14 × 109	W18 × 60
	2	W14 × 176	W24 × 76
	1	W14 × 176	W24 × 84

Floor slabs are composed of 82.5-m (3.25-in.) thick lightweight concrete over 50.8-mm (2-in.) thick steel deck. Seismic mass properties were calculated from anticipated gravity loads on the floors and roof, which include: self-weight of framing, floor/roof dead loads computed from slabs = 2.01 kPa (42 psf); superimposed floor dead load = 1.1 kPa (23 psf); superimposed roof dead load = 1.2 kPa (25 psf); and exterior cladding load = 0.96 kPa (20 psf). For the conventional building, the computed seismic weights are 8561, 8532, and 8922 kN (1924, 1918, and 2005 kips) at the first, second and roof floor, respectively. For the isolated building, the computed seismic weights are 7765, 8085, 8063, and 8728 kN (1745, 1817, 1812, and 1962 kips) at the base, first, second, and roof floors, respectively.

The design displacement D_D of the isolators in the design earthquake and the maximum displacement D_M in the MCE at the center of rigidity are computed as (ASCE 2005):

$$D_D = \frac{gS_{D1}T_D}{4\pi^2 B_D}, \qquad D_M = \frac{gS_{M1}T_M}{4\pi^2 B_M} \tag{1}$$

where T_D, T_M = effective isolation periods; B_D, B_M = coefficients that modify the spectrum for damping; and S_{D1}, S_{M1} = 1-s spectral accelerations for the corresponding events. Target values of $T_M = 3.07$ s and effective damping ratio $\beta_M = 16\%$ were chosen for the MCE, whereas design values T_D and β_D were determined by iteration (Table 2). The total isolator displacement in Table 2 accounts for displacement amplification attributable to accidental torsion (Eq. 17.5-5 and 17.5-6 of ASCE 2005). The isolation

Table 2. Design Parameters for the Isolation Systems

Isolator properties	Design earthquake	MCE
Effective period (s)	$T_D = 2.77$	$T_M = 3.07$
Effective damping (%)	$B_D = 24.2$	$B_M = 15.8$
Isolator displacement [cm (in.)]	$D_D = 32.1$ (12.7)	$D_M = 61.7$ (24.3)
Total displacement [cm (in.)]	$D_{TD} = 38.8$ (15.3)	$D_{TM} = 74.6$ (29.4)

devices have not been designed in detail so that the study is neutral with respect to isolation system. The isolated building does not qualify for design exclusively by the equivalent lateral force method because $S_1 > 0.6$ g and the MCE effective period $T_M > 3.0$ s (ASCE 2005).

Modeling Assumptions

Models for evaluation were based on ASCE 7 (ASCE 2005) for design of new buildings and ASCE 41 (ASCE 2007) for evaluation of existing buildings. Detailed three-dimensional (3D) numerical models of both buildings were developed in OpenSees. Although the buildings are symmetric about both axes, the mass centers were shifted by 5% of the longest plan dimension in both directions to account for accidental torsion (ASCE 2005). Equivalent mass and rotational inertia were lumped at the center of mass. Slab action was accounted for through a rigid diaphragm constraint, except at the base level of the isolated IMRF, where slabs were modeled with shell elements to enhance the rigidity of the model against local isolator uplift.

Member capacities were based on the expected yield strength of structural steel $f_{ye} = 379$ MPa (55 ksi) rather than the nominal design strength (ASCE 2007). All columns and moment-resisting beams were modeled using force-based nonlinear beam-column elements that combine finite length "plastic hinge" regions at the element ends with an interior elastic region (Scott and Fenves 2006). The columns were modeled using fiber sections that inherently account for moment-axial force interaction at each analysis step, whereas stress resultant models were chosen for the moment-resisting beam elements. The steel stress-strain and moment-curvature relationships were assumed to be bilinear, with a strain hardening ratio of 3%. Gravity beams were modeled using elastic frame elements with moment releases at both ends. In the SMRF, moment-resisting and gravity columns were fixed and pinned at the base, respectively; whereas in the IMRF, moment connections were assumed at all base level beam-column joints.

Energy dissipation was applied to the conventional structure and the isolated superstructure using stiffness proportional damping calibrated to give 2.5% damping at their respective first mode frequencies. Stiffness proportional damping was selected since Rayleigh damping has been observed to artificially suppress the first mode of an isolated building even compared with a rigid structure approximation (Ryan and Polanco 2008). Stiffness proportional damping in conventional buildings might be expected to suppress higher mode response. However, damping comparison studies of the SMRF subjected to large intensity ground motions indicated only a trivial difference in median responses between Rayleigh damping and stiffness proportional damping (less than 2% discrepancy in the median peak interstory drift ratio), which allowed this concern to be dismissed. Tangent stiffness proportional damping rather than initial stiffness proportional damping was selected to prevent the damping forces from becoming unrealistically large compared with the element forces after the superstructure yields (Hall 2006; Charney 2008).

The final analytical models for assessment were developed in stages through a series of increasingly complex models that were verified for accuracy. For each building, a basic centerline model of the moment-resisting frame system was developed first, referred to as M1. Next, in model M2, rotational springs were incorporated to model panel zone behavior, coupled with rigid end offsets to account for clear length dimensions of beams and columns (FEMA 2000a). Centerline models and panel zone models are recognized to have the same stiffness in the linear range. Finally, for the conventional SMRF only, a multielement approach was used to simulate the behavior of RBS (model M3). Thus, the response assessment was performed with M3 for the SMRF and M2 for the IMRF.

Panel Zone Flexibility

Panel zones exhibit desirable hysteretic behavior characterized by considerable strain hardening following yielding and stable hysteresis loops. Several mathematical models for panel zone shear force-shear strain (V-γ) relationships have been proposed (Krawinkler 1978; Lu et al. 1988; Tsai and Popov 1988; Kim and Engelhardt 2002). This study utilizes rotational springs that simulate trilinear force-strain behavior (Fig. 2) (Krawinkler 1978; FEMA 2000a). The control values for yield force V_y, plastic force V_p, yield stain γ_y, and plastic strain γ_p are given by:

$$V_y = 0.55 f_{ye} d_c t_w \qquad V_p = V_y \left(1 + \frac{3 b_{cf} t_{cf}^2}{d_b d_c t_w}\right) \tag{2a}$$

$$\gamma_y = \frac{f_{ye}}{\sqrt{3}G} \qquad \gamma_p = 4\gamma_y \tag{2b}$$

where d_c = column depth; b_{cf} = column flange width; d_b = beam depth; t_w = web thickness; t_{cf} = column flange thickness; and G = shear modulus. The elastic stiffness K_e and the postyield stiffness K_p are calculated as the slopes from 0 to yield force V_y and from V_y to the plastic capacity V_p, respectively. Beyond the plastic capacity, mild hardening is represented by a slope of αK_p with $\alpha = 0.03$ (Fig. 2). To implement the rotational springs, the shear strain γ = the rotation angle, and the panel zone shear V is related to ΔM (the net moment transferred to the connection) according to:

$$V = \frac{\Delta M}{d_b} \tag{3}$$

Reduced Beam Section

The RBS approach was developed as an improved approach following the unexpected brittle failures of steel moment frame connections in the Northridge earthquake, and is now used extensively (Foutch and Yun 2002; FEMA 2000b). In the RBS configuration, portions of the beam flanges at a section away from the beam end

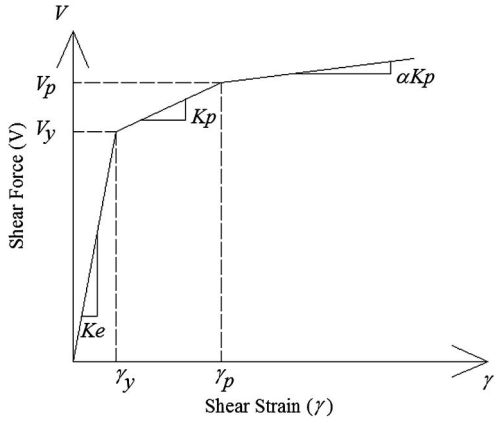

Fig. 2. Panel zone force-deformation behavior

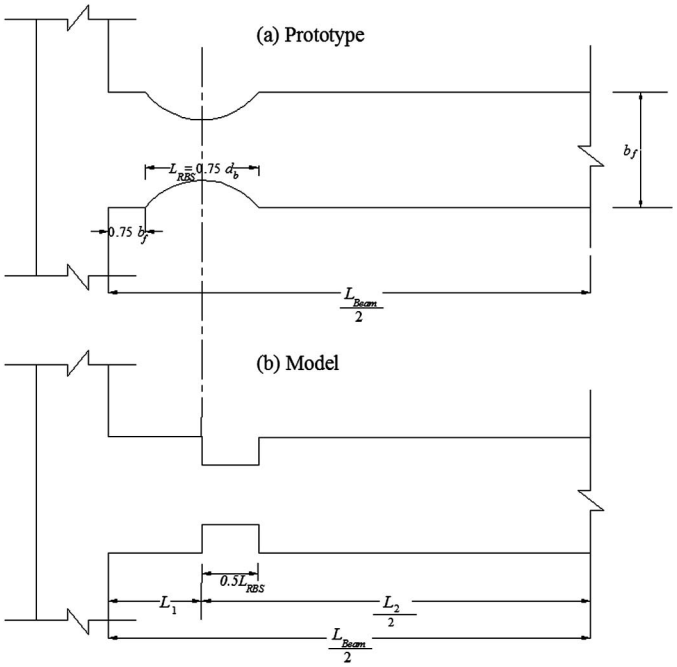

Fig. 3. (a) Plan view with typical geometry for RBS; (b) 3-element frame model; b_f = width of flanges and d_b = beam depth (not shown in plan view)

are tapered. This approach has been observed to effectively eliminate brittle fractures by transferring the zone of plasticity away from the column (Lee and Foutch 2002; FEMA 2000b), as well as improve the overall ductility capacity of the beam-to-column assembly (Shen et al. 2000).

The typical geometry of a circular RBS is depicted in Fig. 3(a); half of the beam is drawn because of symmetry. The flange is tapered starting $3b_f/4$ (b_f = beam flange width) from the face of the column over a length $3d_b/4$, and the flange width is reduced by up to 50% in the middle of the taper. Beams incorporating RBS were modeled with three elements. Elastic frame elements were assigned at the beam ends over length L_1 from the column face to the center of the taper [Fig. 3(b)]. A nonlinear beam-column element with length L_2 was assigned over the remaining interior, with plastic hinge regions over half of the total taper at both ends. Although the section properties vary throughout the tapered region, both the moment capacity and the stiffness of the model were assumed to equal the values computed by section moment-curvature analysis at the midpoint of the taper throughout the plastic hinge region [Fig. 3(b)].

Isolator Model

Isolators were modeled independently, one beneath each column, using a combination of elements to realize a composite force-deformation in each direction that could represent either elastomeric or friction pendulum devices. An elastic column element and an elastic-perfectly plastic spring were assembled in parallel [Fig. 4(a)] to obtain the composite bilinear lateral force-deformation behavior shown in Fig. 4(b). The characteristic yield strength Q, postyield stiffness k_b, and yield displacement u_y of the isolators [Fig. 4(b)] determine the lateral force-deformation relation. Assuming $u_y = 1$ cm, Q and k_b were determined by matching the secant stiffness k_M and hysteretic energy dissipated to the equivalent period $T_M = 3.07$ s and damping ratio $\beta_M = 15.8\%$ at the MCE displacement $D_M = 62$ cm (24.3 in.) (Table 2) according to:

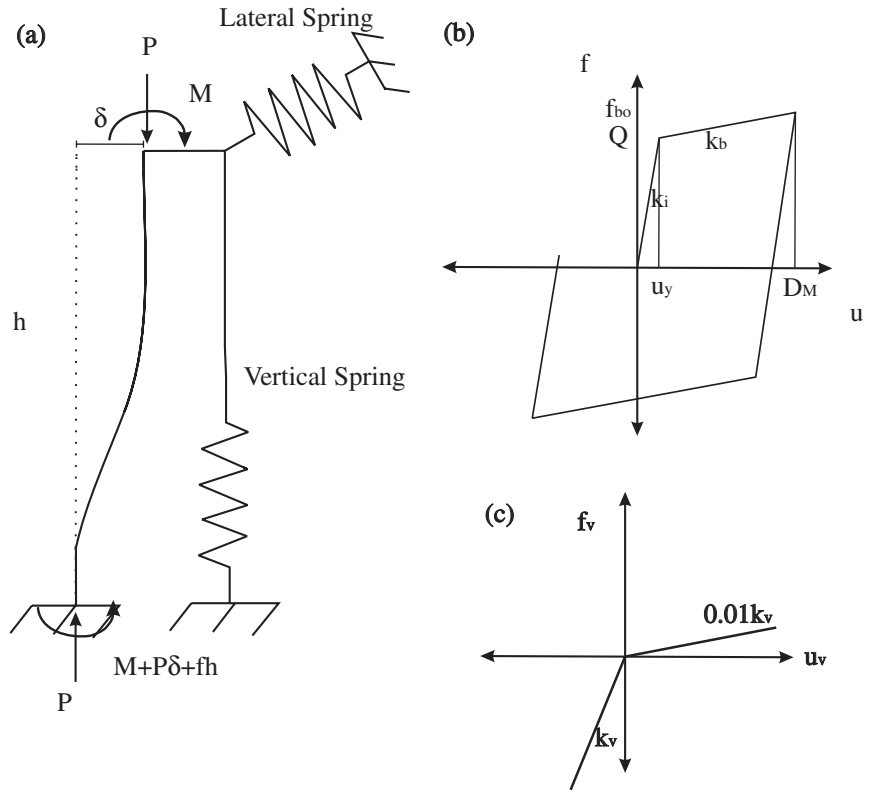

Fig. 4. (a) Isolator model composed of an elastic column element in parallel with lateral and vertical springs; (b) lateral force-deformation; (c) vertical force-deformation in the isolation devices

Table 3. Fundamental Periods of Each Model

	Conventional (SMRF)				Base-isolated (IMRF)	
Period (s)	M1	M2	M3	Mode	M1 and M2	Mode
T1	0.76	0.81	0.83	Lateral torsional	3.21	Lateral torsional
T2	0.74	0.79	0.81	Bidirectional lateral	2.99	Bidirectional lateral
T3	0.49	0.52	0.54	Torsional	2.59	Torsional

$$Q = \frac{\pi k_M \beta_M D_M^2}{2(D_M - u_y)} \tag{4}$$

$$k_b = k_M - \frac{Q}{D_M} \tag{5}$$

The elastic-perfectly plastic spring, with stiffness k_i-k_b and yield strength Q, is a bidirectionally coupled element with a circular yield surface that exhibits identical resistance in any direction in the x-y plane. The column allows transfer of the approximate moments that arise attributable to the lateral deformation of the isolator. For the column element, EI was selected to obtain a lateral stiffness k_b, and the effective height h' was selected such that the moment in the element fh' equals the moment $fh + P\delta$ in the isolator at the design displacement.

Likewise, the composite vertical force-deformation behavior [Fig. 4(c)] was built from the axial stiffness of the column element acting in parallel with a compression-only vertical spring [Fig. 4(a)]. The compressive stiffness k_v of the isolators was computed assuming a vertical frequency of 10 Hz. Since typical bearings have no or low resistance to tension, the tensile stiffness was assumed to be 1% of the value of the compressive stiffness, and EA for the column element was calibrated to a stiffness of $0.01k_v$. The energy dissipation is provided by hysteresis in the lateral directions and 5% viscous damping in the vertical direction at 10 Hz.

Fundamental Properties

Eigenvalue analysis was carried out on the various building models to evaluate their elastic dynamic properties. For eigenvalue analysis, the isolators were modeled as linear springs with stiffness corresponding to the design period $T_D = 2.77$ s. The first three elastic periods and the corresponding deformation modes of each model are listed in Table 3. The fundamental periods using centerline (M1) and panel zone (M2) assumptions are approximately the same, whereas the RBS model (M3) adds flexibility to the conventional building. The first three natural periods of the isolated building are dominated by the isolation system flexibility, but the moderate lengthening of the fundamental period of the isolated building relative to T_D suggests that structural participation in the fundamental mode is nonnegligible. The fundamental $T \approx 1.5$ s for the IMRF superstructure, obtained from a model fixed at the base without the isolators, and thus isolation lengthens the period by less than a factor of 2.

Nonlinear static analysis (or pushover analysis) was carried out under an inverted triangle load pattern to determine the base shear capacity and postyield behavior on the basis of the various building models. Capacity curves for both the conventional SMRF and superstructure of IMRF (fixed without isolators) are plotted in Fig. 5. The panel zone springs (M2 model) and RBS (M3 model) both lead to reduced base shear capacity. The conventional SMRF has a base shear capacity $V \approx 0.65W$ (M3 model), whereas the isolated IMRF has a base shear capacity $V \approx 0.2W$ (M2 model). The predicted ultimate strength computed by energy methods (rigid plastic analysis) is $V = 0.772W$ for the SMRF and $0.264W$ for the IMRF, which correspond closely to the observed values for the M1 model (Fig. 5). Whereas the SMRF model has positive incremental stiffness over the entire postyield range, the IMRF capacity curve essentially flattens after complete yielding. Thus, the isolated IMRF may be more prone to large inelastic excursions in yielding events.

The required minimum design strength coefficients for the SMRF and isolated IMRF were computed as

$$C_{s,\text{SMRF}} = \frac{S_{D1}}{TR} \qquad C_{s,\text{IMRF}} = \frac{V_s}{W} = \frac{k_D D_D}{R_I W} \tag{6}$$

where k_D = secant stiffness of the isolators corresponding to the design period T_D and seismic weight $W = 32{,}641$ kN (7,336 kip) above the isolated base; and the other parameters have been defined. $C_{s,\text{SMRF}} = 0.157$, assuming a natural period of $T = 0.59$ s (Eq. 12.8-7, ASCE 2005); and $C_{s,\text{IMRF}} = 0.10$ on the

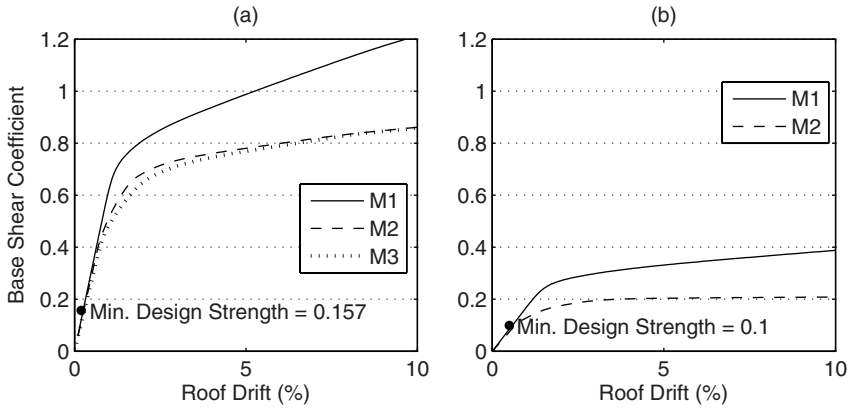

Fig. 5. Capacity curve: (a) conventional building; (b) base-isolated building, with design strength indicated

basis of $V_s = k_D D_D / R_I = 3{,}306$ kN (743 kip). The SMRF is observed to be at least three times stronger than the IMRF, mostly because the SMRF has more overstrength. The design of both buildings is drift-controlled; however, the code factor C_d by which elastic drift is amplified is 5.5 for the SMRF and only 1.67 (equal to R_I) for the IMRF. Thus, considering the effects of overstrength, the ductility based $R \approx 2$ for the SMRF and 1 for the IMRF, suggesting that the observed level of yielding in the two structures is closer than expected.

Ground Motions

The following general procedure was used to select ground motions for different earthquake scenarios (ATC 2009a). First, a hazard curve was defined that quantifies ground motion intensity versus frequency of occurrence, and individual points along the hazard curve represent earthquake scenarios ranging from frequent to rare events. For three distinct earthquake scenarios, target spectra were generated and ground motions were selected and amplitude scaled to best match the target spectra. USGS national seismic hazard maps (Frankel et al. 2000) were consulted to generate uniform hazard spectra (target spectra) for the three selected events: 50% probability of exceedance (PE) in 50 years (50/50), 10% PE in 50 years (10/50), and 2% PE in 50 years (2/50), which correspond to 72, 475, and 2,475-year return periods, respectively. The target spectra list spectral ordinates at periods $T = 0.1$, 0.2, 0.3, 0.5, 1.0 and 2.0 s. Values at 0.2 and 1.0 s for the 2/50 event correspond to S_S and S_1 values for the MCE.

The target spectra are based on a reference shear wave velocity $V_s = 760$ m/s (2,493 ft/s), and were thus modified to reflect the assumed site conditions—site class D with V_s from 180 to 360 m/s (591 to 1,181 ft/s). To modify the target spectra, spectral site modification factors that depend on both ground motion intensity and period were developed from next generation attenuation (NGA) relations (e.g., Campbell and Bozorgnia 2008; Chiou and Youngs 2008). This approach is consistent with site modification factors F_a and F_v used in building codes but reflects the additional periods accounted for in the target spectra. Specifically, site factors were computed as the ratios of spectral acceleration at 760 m/s (2,493 ft/s) and 270 m/s (886 ft/s), with all other factors held constant. Site factors were restricted not to fall below 1.0, even in the short period range. The target spectra for each event are plotted in Fig. 6.

Using USGS seismic deaggregation data (Frankel et al. 2000), ground motions were selected according to the percentage contribution of magnitude and distance pairs to the seismic hazard for a given scenario, which was determined by averaging the deaggregation data over the various periods. For each hazard level, 20 recorded natural ground motions that conform to the magnitude, distance, and site class were selected from the Pacific Earthquake Engineering Research Center (PEER) NGA database (Chiou et al. 2008). Each pair of records was amplitude scaled by a common factor that minimized the difference of the mean spectrum of the components and the target spectrum in the least square sense from $T = 0$ to 3 s. The selection and scaling procedures were based on a range of periods, since the motions were applied to buildings with significantly different fundamental periods.

For the 2/50 and 10/50 hazard levels, the median spectra of the initial 20 pairs of ground motions selected and scaled as previously described were observed to fall well short of the target spectra, particularly in the long period range. Although using recorded ground motions was considered to be ideal, some of the recorded motions were replaced with frequency modified motions to obtain a better match between the target hazard spectra and the median response spectra in the long period range. Hence, 10 pairs of ground motions at the 2/50 and 10/50 hazard levels were replaced by the corresponding SAC steel project—Los Angeles (SAC-LA) ground

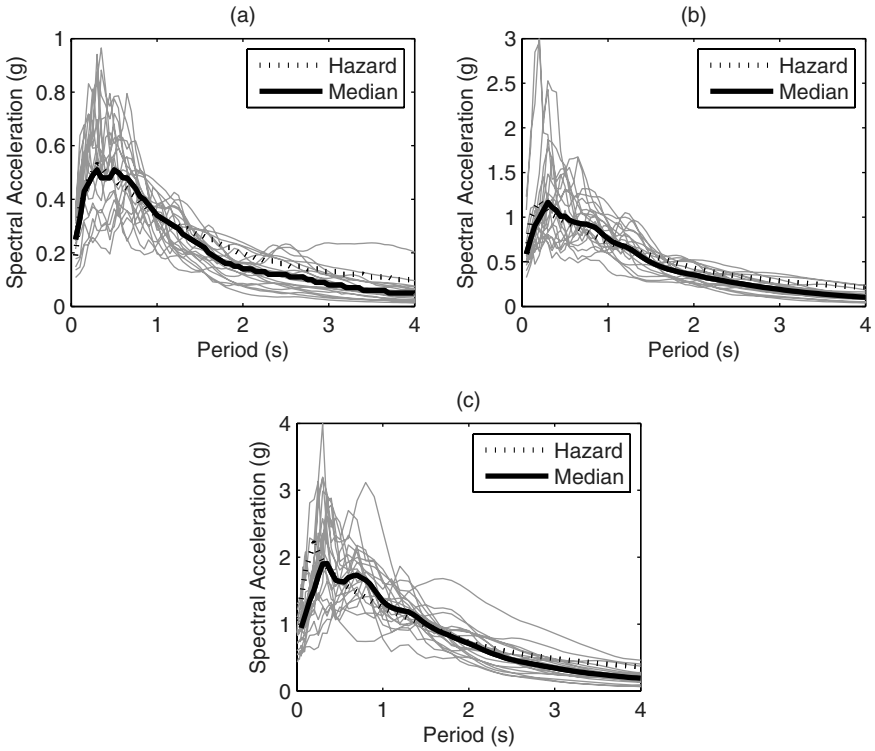

Fig. 6. Acceleration spectra for individual scaled motions, along with median and target spectra: (a) 50/50; (b) 10/50; (c) 2/50 year earthquake scenarios

motion sets. These SAC motions were originally selected for similar location and site conditions and frequency modified to match the target spectra (Somerville et al. 1998).

The ground motions selected for the nonlinear response history analyses for the 50/50, 10/50, and 2/50 events, respectively, are listed on the Network for Earthquake Engineering Simulation (NEES) TIPS project website (NEES 2009). Fig. 6 compares 5% damped acceleration spectra (mean of the x and y components) of the 20 pairs of scaled motions along with their median with the target spectra for each hazard level. A large variance in spectra for individual motions relative to the median is observed. In particular, each hazard level includes some motions with peak accelerations that are 2–3 times the target values at high frequencies. The 2/50 event contains at least one motion with very large spectral accelerations in the long period range [Fig. 6(c)]. However, for all hazard levels, the median spectrum falls somewhat short of the target spectrum beyond $T = 1.5$ s despite the introduction of frequency modified motions.

Comparative Results of Nonlinear Response History Analysis

Nonlinear response history analyses (RHA) were carried out to comparatively evaluate the structural response of the conventional SMRF and isolated IMRF when subjected to the ground motion suites described previously. The statistical distribution of various response quantities for 2/50, 10/50, and 50/50 year events are presented. The selected response quantities include peak and residual story drift ratio, peak total floor acceleration, local element (beam, column, and panel zone) plastic rotations, and isolator deformations (lateral and vertical). Story drift ratios indicate damage to structural elements and drift-sensitive nonstructural components, whereas floor accelerations indicate damage in acceleration sensitive nonstructural components and contents. Plastic rotation demands of individual elements can more precisely indicate local damage, and residual drift criteria determine the threshold between restoring and demolishing a damaged building.

Seismic responses, when sampled over many ground motions, are widely accepted to be lognormally distributed. As such, the median $\hat{x}$ and dispersion δ of the lognormal data were generally used to describe the central tendencies and variability of the response quantities for different ground motion sets. They were computed as

$$\hat{x} = \exp\left[\frac{\sum_{i=1}^{n} \ln x_i}{n}\right] \qquad \delta = \left[\frac{\sum_{i=1}^{n} (\ln x_i - \ln \hat{x})^2}{n-1}\right]^{1/2} \tag{7}$$

However, statistical evaluation on the basis of lognormal distribution [Eq. (7)] is not valid when the sampling set contains zeros, as is the case for plastic rotations. Thus, arithmetic mean μ and standard deviation σ

$$\mu = \frac{\sum_i x_i}{n} \qquad \sigma = \sqrt{\frac{\sum_i (x_i - \hat{x})^2}{n-1}} \tag{8}$$

valid for a normal distribution, were used to describe central tendency and variability of the plastic rotation demands. The 84th percentile values were computed as $\hat{x}\exp(\delta)$ when used with Eq. (7) and $\mu + \sigma$ when used with Eq. (8).

To summarize, the aforementioned statistics are presented in Fig. 7 for peak story drift, Fig. 8 for peak floor acceleration, and Fig. 9 for plastic rotations in beams/panel zones. Selected responses for individual motions are presented in Fig. 10 for the 2/50 year event, such as residual drifts and isolator deformations [Figs. 10(c) and 10(f)], which were negligible in the other events. Statistics on various isolator deformation demands are presented in Table 4. Story drifts were evaluated separately in each direction as the maximum at any of the four corners of the building. Total floor

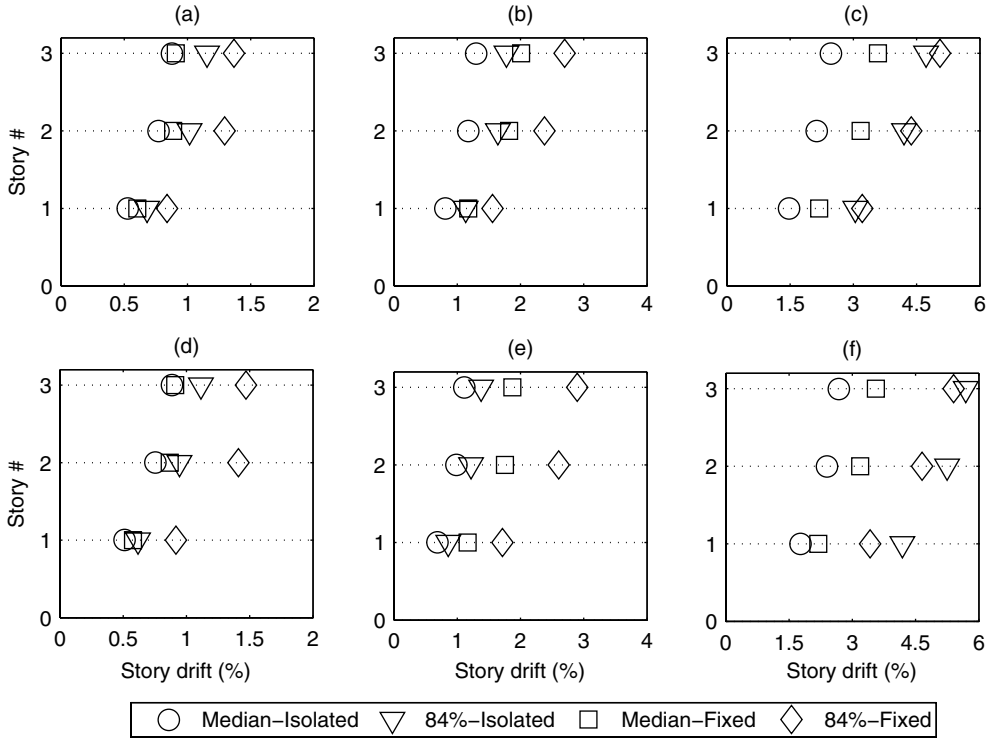

Fig. 7. Story drift ratio demands for: (a)-(c) 50/50, 10/50, and 2/50 year events, respectively, in x-direction; (d)-(f) 50/50, 10/50, and 2/50 year events, respectively, in y-direction

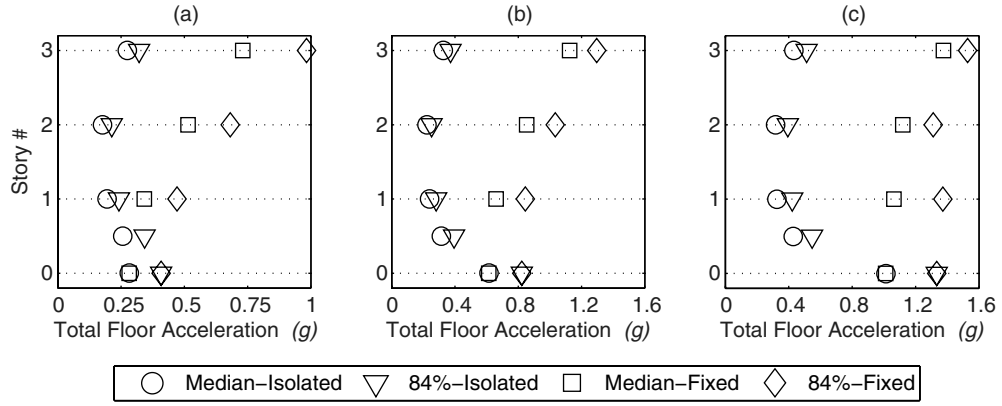

Fig. 8. Total floor acceleration demands: (a) 50/50; (b) 10/50; (c) 2/50 year events

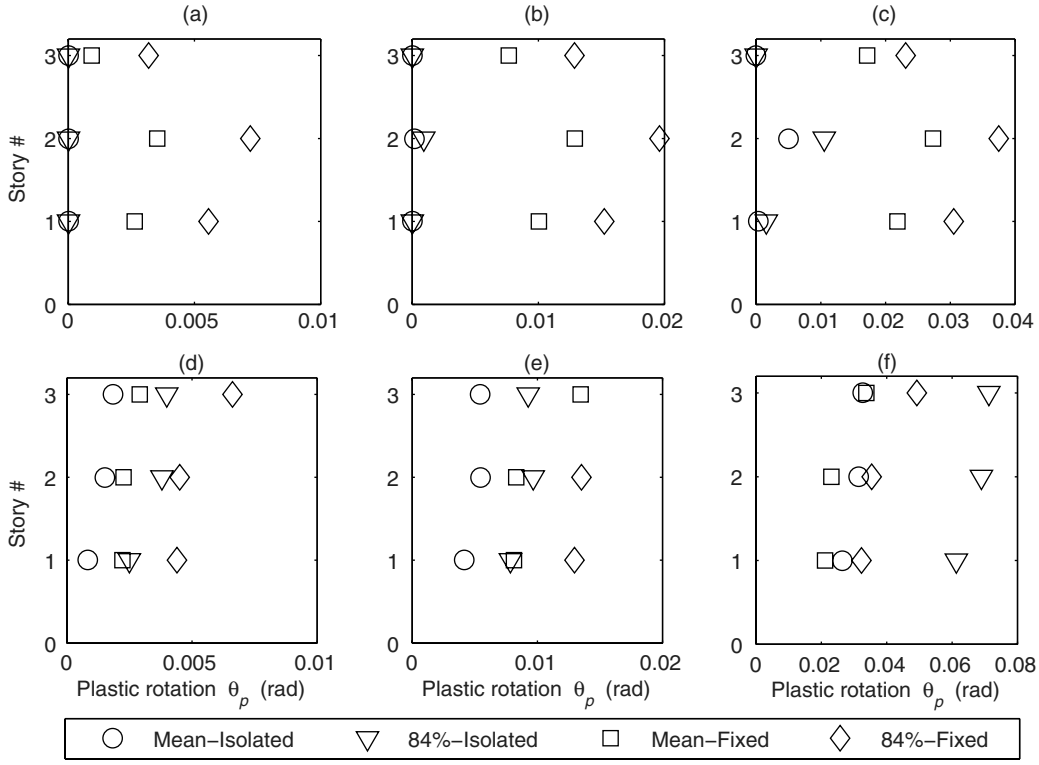

Fig. 9. Beam plastic rotation demands for: (a) 50/50; (b) 10/50; (c) 2/50 year events; and panel zone plastic rotation demands for: (d) 50/50; (e) 10/50; (f) 2/50 year events

acceleration at the center of mass and isolator deformations (maximum over all devices) were evaluated as the vector sums of the demands in the x and y directions. Plastic rotation demands were evaluated as the maximum over all pertinent elements at the given level. When multiple locations or elements were considered, statistics reflect the median (mean) of the local maxima, which may occur at different locations/elements for different ground motions.

Response in Design (10/50 Year) and Frequent (50/50 Year) Events

Although not explicitly identified in building codes, typical design objectives for an isolated building are to suppress yielding and attenuate accelerations to well below the peak ground acceleration (PGA) in the design (10/50 year) event. Using approximate design principles, yield interstory drifts Δ_y were evaluated as

$$\Delta_y = \frac{\varepsilon_y h}{3}\left(\frac{\alpha h}{d_c} + \frac{L_b}{d_b}\right) \tag{9}$$

where ε_y = yield strain; α = reduction factor of 0.8; h and d_c = story height and depth of the column; and L_b and d_b = length and depth of the beam, which led to yield interstory drift values of 1.2% in the conventional SMRF and 1.5% in the isolated IMRF.

For both the frequent (50/50 year) and design events, the story drift demands in the isolated IMRF are below the yield limit of 1.5% [Figs. 7(a), 7(b), 7(d), and 7(e)], with the exception of the 84th percentile in the design event. Beam plastic rotation demands are essentially zero [Figs. 9(a) and 9(b)]. The conventional SMRF

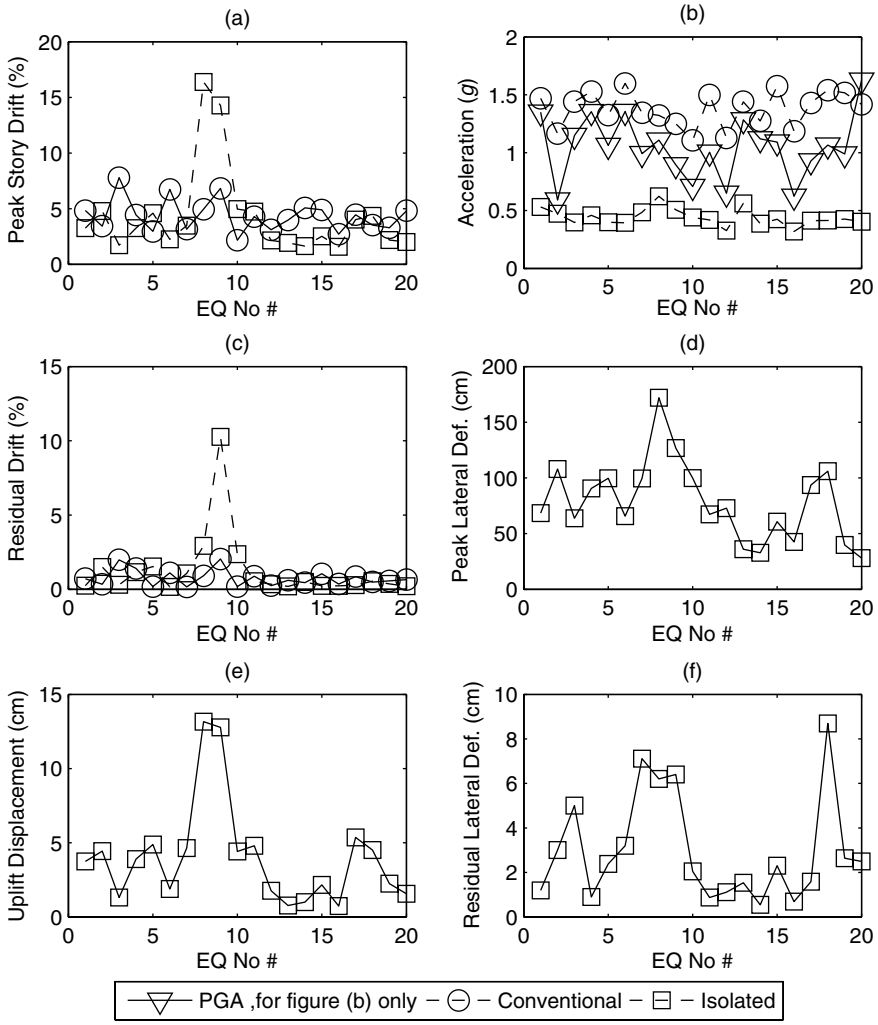

Fig. 10. (a) Peak story drift (%); (b) PGA and roof acceleration; (c) maximum residual story drift; (d) peak isolator deformation; (e) peak isolator uplift; (f) maximum residual isolator deformation sampled for individual motions in the 2/50 year event

more certainly yields in the design event, with median story drift demands around 2% in stories 2 and 3 [Figs. 7(b) and 7(e)], and median beam plastic rotation demands from 0.01 to 0.015 rad in floors 1 and 2 [Fig. 9(b)]. In the frequent event, the conventional SMRF is on the verge of yielding, with median story drifts around 1.2% [Fig. 7(a)] and accumulated beam plastic rotations around 0.004 rad. Column plastic rotation demands (not shown) were generally close to zero everywhere in both buildings. Column plastic rotations occur only at the base of the conventional SMRF in the design and larger events, thus the capacity design concept effectively prevents column yielding and soft story mechanisms. Minor panel zone yielding is observed in the isolated IMRF for the design and even frequent events [Figs. 9(d) and 9(e)]. AISC 341 (2005) intends that panel zone yielding should not precede hinge formation in an SMRF; however, the same criteria do not apply to systems detailed as IMRF, which could explain why the panel zone yielding occurs even in relatively small events. It may be desirable to further examine the IMRF design criteria for isolated buildings. Although minor instances of yielding are observed in the design event, the design objectives could be interpreted as having been met or nearly met.

Table 4. Peak and Residual Isolator Displacement Demands

Scenario	Statistics	Peak isolator displacement [cm (in.)]	Residual isolator displacement [cm (in.)]
50 in 50	Median	11.48 (4.52)	1.73 (0.68)
	84%	20.19 (7.95)	2.87 (1.13)
10 in 50	Median	35.04 (13.79)	1.60 (0.63)
	84%	54.12 (21.31)	3.12 (1.23)
2 in 50	Median	70.82 (27.88)	2.21 (0.87)
	84%	115.19 (45.35)	5.00 (1.97)

With respect to accelerations, the median roof acceleration in the isolated IMRF is attenuated by a factor of almost 2 (PGA = 0.61 g and roof acceleration = 0.33 g) in the design event [Fig. 8(b)]. However, the median roof acceleration demand in the conventional SMRF is amplified to 1.15 g for the same event. The accelerations at level 0 (ground) designate PGA and the accelerations between 0 and 1 designate accelerations just above the isolators (Fig. 8). The design objectives for acceleration in the IMRF have certainly been met.

For the design and frequent events, the demands in the isolated building can be predicted with high confidence as the dispersions (reflected in the difference between median and 84th percentile responses) in story drifts and especially total floor accelerations are quite small [Figs. 7(a), 7(b), 7(d), 7(e), 8(a), and 8(b)]. Since the isolated IMRF responds close to elastically, the dispersion in story drift is limited relative to the conventional SMRF. Regarding

floor accelerations, extreme values (high or low) of PGA are observed not to correlate well with extreme values of roof acceleration in the isolated IMRF, as shown plotted for each ground motion [Fig. 10(b)] for the 2/50 year event (MCE), where limited dispersion was also observed [Fig. 8(c)]. One possible explanation for the small dispersion in acceleration is that period lengthening generally has a smoothing effect on spectral accelerations, which are correlated to floor accelerations.

Although the benefits of seismic isolation are apparent, story drift reduction is somewhat suppressed compared with ideal applications because of the flexibility of the moment frame. For the design event, median story drift demands in the isolated IMRF are reduced on the order of 33–50% relative to the conventional SMRF [Figs. 7(b) and 7(e)], which is small compared with expectations set by pedagogical studies (e.g., Kelly 1997). Although comparative studies often assume comparable natural periods (e.g., Sayani and Ryan 2009), in this study, the IMRF without isolators is substantially more flexible than the conventional SMRF. Furthermore, the effective isolation period ($T_D = 2.77$ s) exceeds the superstructure natural period ($T = 1.5$ s) by less than a factor of 2 at the design displacement. Therefore, significant structural participation in the first mode, leading to moderate story drift demands, is unsurprising. Damage in drift-sensitive nonstructural components is not eliminated in the design event by seismic isolation, as damage to interior partition walls is predicted at median drifts as low as 0.25% (ATC 2009a).

The relative drift reduction is even smaller for the frequent event compared with the design event, wherein median story drift demands are reduced only slightly relative to the conventional SMRF [Figs. 7(a) and 7(d)]. To interpret, the isolation system becomes less effective for earthquake intensities lower than the design event because it is not fully activated [median deformation = 11.48 cm (4.52 in.) (Table 4)], resulting in a higher effective stiffness and a smaller period separation compared with the superstructure. As further evidence, floor accelerations, normally reduced by at least a factor of 2 relative to PGA, are no less than 2/3 of PGA in the frequent event [Fig. 8(a)].

Response in MCE (2/50 Year Event)

Although story drifts for the isolated IMRF are generally reduced in the MCE (2/50 year event) relative to the conventional SMRF, the same confidence in the superior performance of isolation in a design event cannot be extended to the MCE. For example, the median peak story drift is reduced from about 3.6% for the conventional SMRF to about 2.7% for the isolated IMRF, but the 84th percentile story drift demands are comparable in both, if not larger in the IMRF [Figs. 7(c) and 7(f)]. The increase in the 84th percentile drift is the result of outliers; for example, records 8 and 9 induce peak drift demands on the order of 15–16% in the isolated IMRF [Fig. 10(a)]. The residual story drift in the isolated IMRF from record 9 is predicted to be on the order of 11% [Fig. 10(c)], which would almost certainly lead to collapse. Similar outliers are not observed for the conventional SMRF, as several motions induce peak story drifts on the order of 5–8% [Fig. 10(a)] and residual drifts on the order of 1–2% [Fig. 10(c)]. Analysis of the outliers is discussed further in the next section. The isolation system is very effective in limiting total floor accelerations to levels well below the PGA [Fig. 8(c)]. Through the simple force balance concept, structural yielding helps to limit acceleration demands. Thus, acceleration outliers [Fig. 10(b)] or large acceleration dispersions [Fig. 8(c)] are not observed for the isolated IMRF in the MCE.

Several motions in addition to those that have been declared as outliers induce isolator deformation demands beyond those that could reasonably be accommodated by the isolation system, and in such instances the predicted response of the IMRF is unreliable. The median isolator deformation of 70.82 cm (27.88 in.) (Table 4) exceeds the MCE displacement $D_M = 61.7$ cm (24.3 in.) (Table 2), and the 84th percentile deformation of 115.19 cm (45.35 in.) (Table 4) exceeds $D_{\mathrm{TM}} = 74.6$ cm (29.4 in.) (Table 2). Furthermore, the peak isolator deformation exceeds D_{TM} for 9 of 20 ground motions [Fig. 10(d)]. Since the seismic gap length and moat wall location are at the designer's discretion, the potential collision with a moat wall was not simulated in this study. However, under reasonable design practices, collisions with the outer moat wall would be expected for some of the ground motions considered, and the impact would transmit high-frequency waves through the superstructure that may lead to an increase in drifts and accelerations in the superstructure compared with those predicted in this study.

The uplift displacement demands in isolators, sampled for individual ground motions in Fig. 10(e), are also of concern. The average uplift is around 2.5 cm (1 in.), which would probably be acceptable in design, but exceeds 12.5 cm (5 in.) for two of the ground motions. In reality, different isolation devices manage uplift in a variety of ways that are not well captured in this study.

Residual drift demands in both buildings are usually below 1%, but demands above 2% are induced by a couple of motions for the conventional SMRF and several motions for the isolated IMRF, including one outlier that has already been discussed [Fig. 10(c)]. Residual isolator deformations are generally below 2.5 cm (1 in.), but for a few records, fall between 5 and 10 cm (2 and 4 in.) [Fig. 10(f)]. As observed previously, drift demands are somewhat comparable in both buildings [Figs. 7(c) and 7(f)]. Beam plastic rotations are the source of large drifts for the conventional SMRF [Fig. 9(c)], whereas panel zone plastic rotations are the source of large drifts for the isolated IMRF [Fig. 9(f)]. Beam rotations are larger for the conventional SMRF because the RBS model reduces the beam capacity relative to the panel zone capacity. Even though the relative beam versus panel zone plastic rotations are known to be sensitive to the modeling assumptions, the high panel zone rotation demands in the isolated IMRF, on the order of 0.06–0.07 rad (6–7%) at the 84th percentile, confirms the previous suggestion that the appropriateness of the IMRF panel zone design criteria for use in isolated buildings should be verified. The ductility capacity of the WUF-W connection used in the IMRF is expected to be lower than the RBS connection used in the SMRF, perhaps putting the isolated IMRF at risk of weld fractures in the MCE.

As stated previously, although design objectives could be interpreted as being met, significant performance benefits would likely be seen, especially in the MCE, by stiffening and strengthening the superstructure of the isolated IMRF beyond minimum code compliance. Some California jurisdictions have chosen to exceed International Building Code (IBC) requirements by enforcing a design of $R_I = 1$ in the MCE for nonductile systems, such as IMRF and ordinary braced frames. On the other hand, no amount of strengthening and stiffening would help to control isolator deformations in the MCE. The deformation demands are very susceptible to the ground motions, which are discussed further in the next section.

Discussion of Outliers

The phenomenon of the outlier responses is studied further by analyzing the feasibility of both the isolator deformations and story drifts predicted in the simulation. Recall that the isolation system was designed for a period $T_M = 3.07$ s and damping ratio $\beta_M = 15.8\%$, with a design deformation of 62 cm (24 in.) (Table 2). For the 2/50 year event, 20 ground motion records were selected and scaled such that the mean component spectra (i.e., mean of

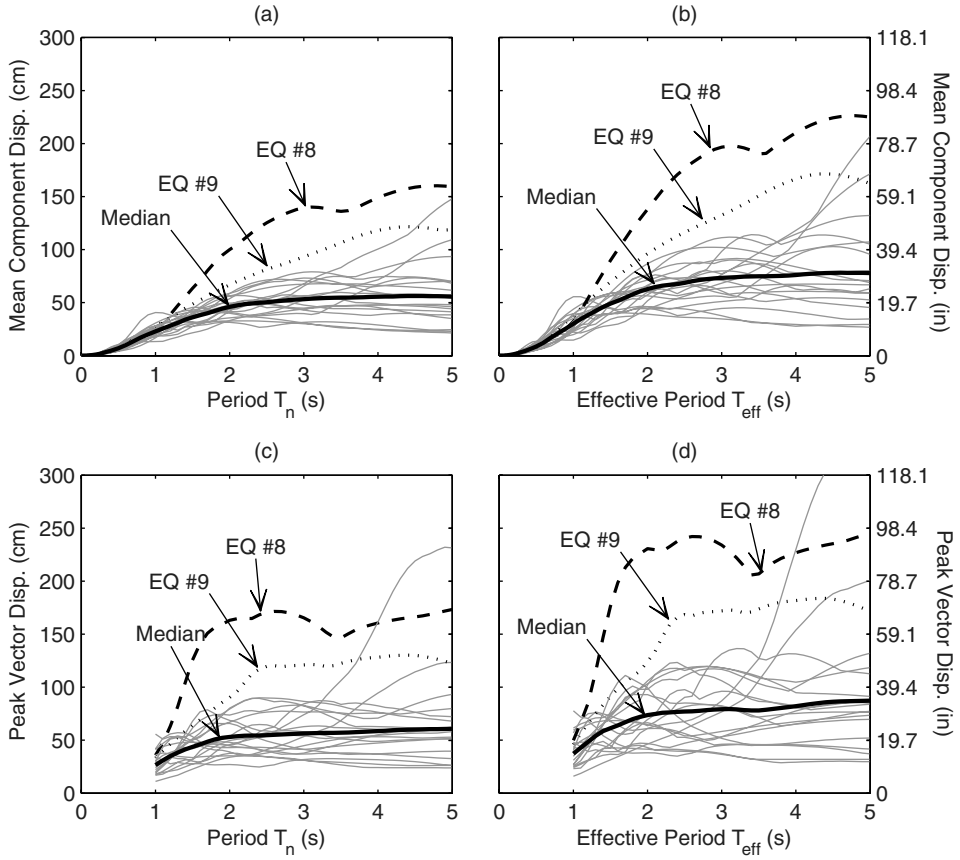

Fig. 11. Spectral displacement for 16% damping for individual records in the 2/50 year event: (a) and (b) mean of x and y-component displacement for a linear system and a bilinear system with given equivalent linear properties, respectively; (c) and (d) peak displacement in any direction for a linear system and a bilinear isolation system with given equivalent linear properties, respectively

x and y-component spectral response) best fit the 5% damped target spectrum. In accordance with the isolation system design parameters, the 16% damped mean component displacement spectra is shown in Fig. 11(a) for individual records, along with the median over the 20 records. At a period $T_n = 3.1$ s, the median displacement is about 53 cm (21 in.), which is below the MCE displacement target of 62 cm (24 in.), consistent with the target spectra in Fig. 6(c). The mean component displacement falls between 25 and 76 cm (10 and 30 in.) for 18 of 20 motions, but records #8 and #9 have higher displacements of 140 and 94 cm (55 and 37 in.), respectively.

However, the isolation system is not linear as assumed, but bilinear, with parameters selected to match equivalent period and damping ratio at the target displacement. As a net result of the nonlinearity, the median displacement increases slightly [from 53 to 56 cm (21 to 22 in.) at 3.1 s], and the displacement of the outliers increases by a lot [from 140 to 163 cm (55 to 64 in.) for record #8 and from 94 to 122 cm (37 to 48 in.) for record #9] [Fig. 11(b)].

Finally, the relevant displacement for the isolation system is not the mean component displacement but the peak displacement in any direction, which is a vector sum of the two components at each time step. The peak vector spectral displacement is illustrated in Fig. 11(c) for a linear system and in Fig. 11(d) for a bilinear system with equivalent linear properties. The peak vector displacement is observed to increase significantly compared with the corresponding mean component displacement. For a bilinear system [Fig. 11(d)], the median displacement at 3.1 s is 79 cm (31 in.), and the displacement is between 36 and 112 cm (14 and 44 in.) for 18 of 20 motions. On the basis of Fig. 11(d), the expected peak isolator displacements attributable to records #8 and #9 have increased to 229 and 171 cm (90 and 67 in.), respectively.

The code Equivalent Lateral Force Procedure (ELFP) does not directly account for bidirectionality or the discrepancy between linear and nonlinear (equivalent linear) response. The dynamic procedures (response spectrum and response history analysis) have more direct procedures for incorporating these effects. However, ELFP indirectly includes further increases in MCE displacement/gap width through a torsion factor. Furthermore, the peak isolator deformation observed during dynamic analysis of the 3D building model is reduced compared with that of the bilinear spectral analysis [Fig. 11(d)], which offsets some of the increases not accounted for in the code. This occurs because some of the spectral displacement is carried as interstory drift in the superstructure, especially when the superstructure is as flexible as a moment frame. Consequently, the predicted isolator deformations to records #8 and #9, 175 and 125 cm (70 and 50 in.), respectively, are very plausible.

The next item to explore is what happens to the superstructure when the isolation system experiences a deformation demand of 175 cm (70 in.). The force coefficient f_b/W in the isolators (equal to the base shear coefficient passed to the superstructure) can be found by normalizing the force-deformation curve [Fig. 4(b)] by the weight:

$$\frac{f_b}{W} = \frac{Q}{W} + \frac{\omega_b^2}{g} D \tag{10}$$

where Q is defined in Eq. (4); ω_b = frequency corresponding to k_b [Eq. (5)]; and D = deformation in the isolators. The parameters for

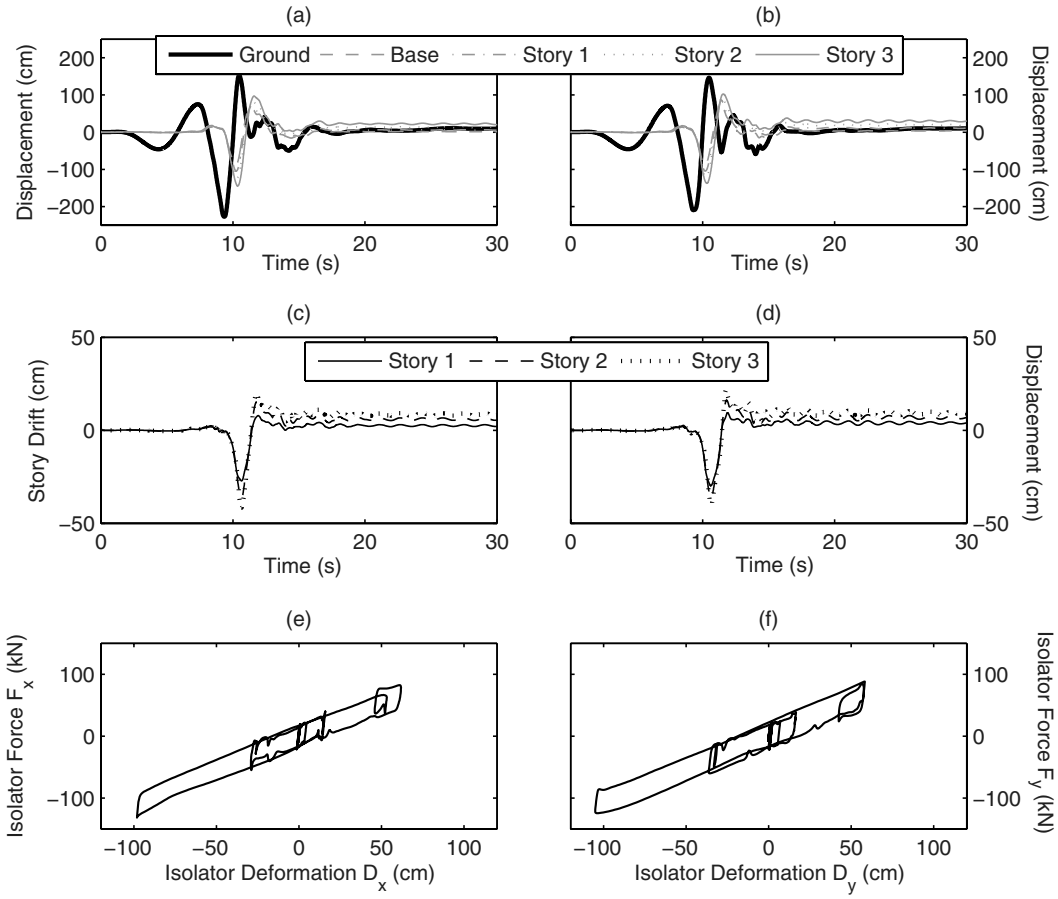

Fig. 12. History of IMRF responses to earthquake record #8: (a), (b) displacements at CM in x and y-directions, respectively; (c), (d) story drifts at top left corner in x and y-directions, respectively; (e), (f) top left corner isolator force-deformation in x and y-directions, respectively

this isolation system, found by solving Eqs. (4) and (5), are $Q/W = 0.066$ and $\omega_b^2 = 3.06$ rad/s. At the MCE displacement of 62 cm (24 in.), the force coefficient $f_b/W = 0.26$ and the push-over analysis of model M2 [Fig. 5(b)] suggest that the superstructure has already yielded. At an isolator displacement of 175 cm (70 in.), nearly three times the MCE displacement, the force coefficient $f_b/W = 0.62$, which implies that the superstructure is subjected to a base shear 2.5 to 3 times its strength, or a force reduction factor $R \geq 2.5$. Under such demands, a conventional long period structure might be expected to follow the equal displacement rule, where ductility demand $\mu = R$. However, a recent study by the authors (Sayani and Ryan 2009) suggests that ductility demand accumulates much faster in an isolated building, and based on the superstructure period, the isolated building could be expected to see a ductility demand on the order of $\mu = 6$ when subjected to $R = 2.5$ [Fig. 3 of Sayani and Ryan (2009)]. With a yield drift demand of 1.5%, $\mu = 6$ could, on average, lead to a peak drift demand of about 9% in a simplistic SDOF structural model. However, considering the added complexities of the 3D model, including accidental torsion, uplift of the isolation system, and the fact that interstory drift demands on average exceed peak roof drift demands, it is credible that the actual peak interstory drift demands for record #8 exceed 15%.

Other studies have also drawn conclusions that help confirm that outliers occur, e.g., yielding is self-limiting in conventional structures but self-propagating in isolated structures (Kikuchi et al. 2008), and isolated buildings are more sensitive than conventional buildings to statistically reasonable uncertainties in ground motions (Politopoulos and Sollogoub 2005).

Select response histories of the IMRF to record #8 are shown in Fig. 12, including displacements of center of mass (CM) in x and y-directions [Figs. 12(a) and 12(b)], x and y-direction story drifts sampled at the corner where they were observed to be largest [Figs. 12(c) and 12(d)], and force-deformation of the isolator in x and y-directions, also sampled at the corner where it was observed to be largest [Figs. 12(e) and 12(f)]. From the displacement histories, a large 3 to 4-s pulse of the ground motion with a displacement of about 200 cm in each direction is observed. The building follows suit, wherein each story also carries a large pulse with displacements up to 150 cm [Figs. 12(a) and 12(b)]. Consequently, large story drifts of up to 40 cm are observed; the story drifts shown in Figs. 12(c) and 12(d) are about 30–40% larger than those at the CM. The force-deformation of the isolator resembles a standard bilinear curve with bidirectional coupling; the bidirectional interaction can be seen especially out at the positive deformation limit of about 60 cm. The peak deformation in the isolators shown in Figs. 12(e) and 12(f) falls short of that reported in Fig. 10(d), because the latter reflects a vector displacement, derived as a combination of the components.

The preceding analysis has clearly demonstrated that the isolator deformation demands, and subsequent superstructure response, are very sensitive to the individual ground motions. Both of the declared outliers occurred in simulated motions, which may be considered less likely to occur than motions recorded in previous earthquakes. Nevertheless, finding new and creative ways to limit the deformation demands of the isolators in extreme motions would greatly increase the performance reliability.

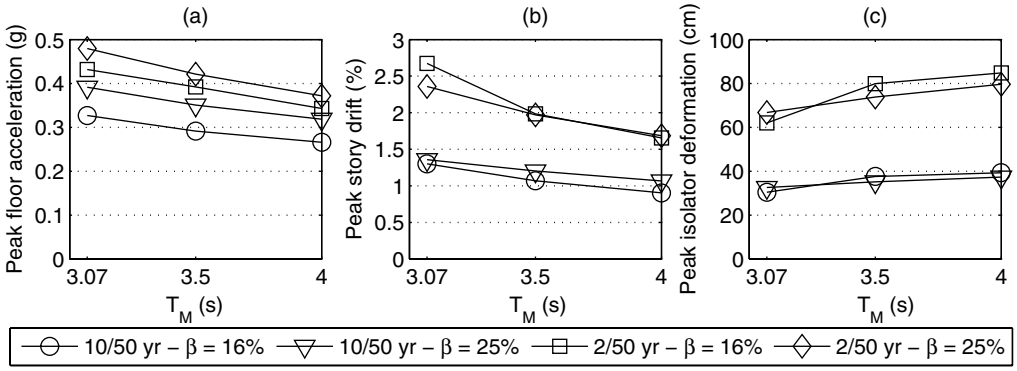

Fig. 13. Median values of: (a) peak floor acceleration; (b) peak interstory drift; (c) peak isolator deformation as a function of isolation system parameters in the 10/50 and 2/50 year events

Influence of Isolation System Parameters

Additional analyses were conducted to understand the influence of isolation system parameters on isolator deformation demands, drift demands, and acceleration demands. In total, the cases that were considered include target period $T_M = 3.07$, 3.5, and 4.0 s, and target damping ratios of $\beta_M = 16$ and 25%, and isolation system properties were chosen according to the procedure described previously. Fig. 13 presents median values of peak floor acceleration, peak story drift, and peak isolator deformation demand anywhere in the structure as a function of isolation period for the 10/50 and 2/50 year events.

As expected, both acceleration demands [Fig. 13(a)] and interstory drift demands [Fig. 13(b)] decrease as the isolation period is increased. Added damping does not have a very significant influence on reducing interstory drifts or isolator deformation demands, and it actually increases acceleration demands. The acceleration demands increase by a large margin in the 10/50 year event when β_M is increased from 16 to 25% [Fig. 13(a)]. Increasing the isolation period from 3 to 4 s results in only a marginal increase in isolator deformation demand for the 10/50 year event but reduces story drifts by 20 to 30%. Accommodating the deformations in the 2/50 year event may definitely prove to be problematic for all cases investigated. Overall, substantive performance benefits are apparent if the isolation period is increased, but accommodating larger deformation demands in the isolation system is often the limiting factor.

Conclusions

The seismic performance of minimally code-compliant 3-story low-rise steel moment frame buildings—both conventional SMRF and base-isolated IMRF—has been compared. Synthesis of the seismic response of the two buildings has led to the following conclusions:

- The design objectives for the isolated IMRF have been basically met, i.e., structural yielding, aside from some minor yielding in the panel zones, is unlikely for both the design (10/50 year) and frequent (50/50 year) events. Floor accelerations are reduced considerably—by factors of 3 or 4—relative to the conventional SMRF for both events.
- Demands in an isolated building can be predicted with high confidence for ground motion intensities at or below the design intensity, as the dispersions in response parameters are reduced to a fraction of those in the conventional building.
- The flexibility of the moment frame leads to nonnegligible structural participation in the first modes of the isolated IMRF and larger relative story drifts compared with idealized (stiff) structural systems. This phenomenon is exacerbated in a frequent/small event where the isolation system is not fully activated. Damage to drift-sensitive nonstructural components may be expected. However, an isolated IMRF provides reliable, stable performance, and floor accelerations are attenuated to values that would safeguard acceleration sensitive nonstructural components and contents.
- In this study, a few extreme ground motions, which had been selected according to industry accepted procedures, induced outlier responses in the MCE (2/50 year event). To exacerbate the problem, the isolator deformation demands are often larger than expected because the Equivalent Lateral Force Procedure does not include an explicit provision to amplify the design displacement for bidirectional coupling effects. Regardless of the outliers, yielding is pervasive in the 2/50 year event because the IMRF has little reserve capacity, and the reduction in drift demands relative to the SMRF is marginal.
- In a design event, elongating the period of the isolation system decreases both drift and acceleration demands with marginal increases in isolator deformation. Increasing the damping of the isolation system reduces drift demands slightly, but increases accelerations by a larger amount.

Given these observations, one might conclude that a minimally code-compliant IMRF design meets typical performance objectives for the design event, but a more robust design is advisable if the response in a rarer earthquake is important. Regardless of the superstructure design, controlling or limiting the isolator deformation demands in the rare (2/50 year) event stands out as an unsolved problem that may require new and creative approaches.

Acknowledgments

This material is based on work supported by the National Science Foundation under Grant No. CMMI-0724208 and the Utah State University College of Engineering. Any opinions, findings, and conclusions or recommendations expressed in this material are those of the authors and do not necessarily reflect the views of the sponsors. The authors recognize the efforts of Forell-Elsesser Engineers with Dr. Troy Morgan for designing the buildings to be analyzed. The authors also wish to thank Professor Stephen Mahin and Dr. Troy Morgan for contributing their technical expertise and offering feedback on the study.

References

Agarwal, V. K., Niedzwecki, J. M., and van de Lindt, J. W. (2007). "Earthquake induced pounding in friction varying base isolated buildings." *Eng. Struct.*, 29(11), 2825–2832.

American Institute of Steel Construction (AISC). (2005). "Seismic provisions for structural steel buildings." *AISC 341-05*, Chicago.

American Society of Civil Engineers (ASCE). (2005). "Minimum design loads for buildings and other structures." *ASCE 7-05*, Reston, VA.

American Society of Civil Engineers (ASCE). (2007). "Seismic rehabilitation of existing buildings." *ASCE 41*, Reston, VA.

Applied Technology Council (ATC). (2008a). "Reducing the risks of nonstructural earthquake damage." *ATC-69 Project Rep.—State of the Art and Practice*, Prepared for Federal Emergency Management Agency, Washington, DC.

Applied Technology Council (ATC). (2009a). *Guidelines for Seismic Performance Assessment of Buildings 50% Complete Draft*, Prepared for Department of Homeland Security, Washington, DC.

Applied Technology Council (ATC). (2009b). "Quantification of building seismic performance factors." *ATC-63 Project Rep., FEMA P695*, Prepared for Federal Emergency Management Agency, Washington, DC.

Building Seismic Safety Council (BSSC). (2004). "NEHRP recommended provisions and commentary for seismic regulations for new buildings and other structures." *FEMA 450*, Washington, DC.

Campbell, K. W., and Bozorgnia, Y. (2008). "NGA ground motion model for the geometric mean horizontal component of PGA, PGV, PGD and 5% damped linear elastic response spectra for periods ranging from 0.01 to 10 s." *Earthquake Spectra*, 24(1), 139–171.

Ceccoli, C., Mazzotti, C., and Savoia, M. (1999). "Non-linear seismic analysis of base-isolated RC frame structures." *Earthquake Eng. Struct. Dyn.*, 28(6), 633–653.

Charney, F. A. (2008). "Unintended consequences of modeling damping in structures." *J. Struct. Eng.*, 134(4), 581–592.

Chiou, B., Darragh, R., Gregor, N., and Silva, W. (2008). "NGA project strong-motion database." *Earthquake Spectra*, 24(1), 23–44.

Chiou, B. S.-J., and Youngs, R. S. (2008). "An NGA model for the average horizontal component of peak ground motion and response spectra." *Earthquake Spectra*, 24(1), 173–216.

Dolce, M., and Cardone, D. (2003). "Seismic protection of light secondary systems through different base isolation systems." *J. Earthquake Eng.*, 7(2), 223–250.

Dolce, M., Cardone, D., and Ponzo, F. C. (2007). "Shaking-table tests on reinforced concrete frames with different isolation systems." *Earthquake Eng. Struct. Dyn.*, 36(5), 573–596.

Federal Emergency Management Agency (FEMA). (2000a). "State of the art report on systems performance of steel moment frames subjected to earthquake ground shaking." *FEMA 355-C*, Washington, DC.

Federal Emergency Management Agency (FEMA). (2000b). " State of the art report on connection performance." *FEMA 355-D*, Washington, DC.

Foutch, D. A., and Yun, S. (2002). "Modeling of steel moment frames for seismic loads." *J. Constr. Steel Res.*, 58(5–8), 529–564.

Frankel, A. D. et al. (2000). "USGS national seismic hazard maps." *Earthquake Spectra*, 16(1), 1–19.

Hall, J. F. (2006). "Problems encountered from the use (or misuse) of Rayleigh damping." *Earthquake Eng. Struct. Dyn.*, 35(5), 525–545.

Hall, J. F., and Ryan, K. L. (2000). "Isolated buildings and the 1997 UBC near-source factors." *Earthquake Spectra*, 16(2), 393–412.

Hamidi, M., El Naggar, M. H., and Vafai, A. (2003). "Response of structures supported on SCF isolation systems." *Earthquake Eng. Struct. Dyn.*, 32(10), 1555–1584.

International Code Council (ICC). (2006). *International Building Code (IBC)*, Falls Church, VA.

Kelly, J. M. (1997). *Earthquake-resistant design with rubber*, 2nd Ed., Springer-Verlag, London.

Kikuchi, M., Black, C. J., and Aiken, I. D. (2008). "On the response of yielding seismically isolated structures." *Earthquake Eng. Struct. Dyn.*, 37(5), 659–679.

Kim, K. D., and Engelhardt, M. D. (2002). "Monotonic and cyclic loading models for panel zones in steel moment frames." *J. Constr. Steel Res.*, 58(5–8), 605–635.

Krawinkler, H. (1978). "Shear in beam-column joints in seismic design of steel frames." *Eng. J.*, 15(3), 82–91.

Lee, K., and Foutch, D. (2002). "Performance evaluation of new steel frame buildings for seismic loads." *Earthquake Eng. Struct. Dyn.*, 31(3), 653–670.

Lin, A. N., and Shenton III, H. W. (1992). "Seismic performance of fixed-base and base-isolated steel frames." *J. Eng. Mech.*, 118(5), 921–941.

Lu, L. W., Wang, S. J., and Lee, S. J. (1988). "Cyclic behavior of steel and composite joints with panel zone deformation." *Proc. 9th World Conf. on Earthquake Engineering*, Vol. IV, International Association for Earthquake Engineering, Tokyo.

Naaseh, S., Morgan, T. A., and Walters, M. T. (2002). "A critical evaluation of current US building code provisions and FEMA guidelines for the design of seismic isolated structures." *Proc. ATC 17-2 Seminar on Seismic Isolation, Passive Energy Dissipation and Active Control*, Applied Technology Council, Los Angeles.

Network for Earthquake Engineering Simulation (NEES). (2009). "Tools for isolation and protective systems (TIPS)." ⟨http://www.neng.usu.edu/cee/faculty/kryan/NEESTIPS/PBEE_study.html⟩ (Jul. 13, 2009).

Ordonez, D., Foti, D., and Bozzo, L. (2003). "Comparative study of the inelastic response of base isolated buildings." *Earthquake Eng. Struct. Dyn.*, 32(1), 151–164.

Palazzo, B., and Petti, L. (1996). "Reduction factors for base isolated structures." *Comput. Struct.*, 60(6), 945–956.

Pinto, P. E., and Vanzi, I. (1992). "Base isolation: Reliability for different design criteria." *Proc. 10th World Conf. on Earthquake Engineering*, Balkema, Rotterdam, Netherlands, 2033–2038.

Politopoulos, I., and Sollogoub, P. (2005). "Vulnerability of elastomeric bearing isolated buildings and their equipment." *J. Earthquake Eng.*, 9(4), 525–545.

Ryan, K. L., and Polanco, J. (2008). "Problems with Rayleigh damping in base-isolated buildings." *J. Struct. Eng.*, 134(11), 1780–1784.

Sayani, P. J., and Ryan, K. L. (2009). "Comparative evaluation of base-isolated and fixed-base buildings using a comprehensive response index." *J. Struct. Eng.*, 135(6), 698–707.

Scott, M. H., and Fenves, G. L. (2006). "Plastic hinge integration methods for force-based beam-column elements." *J. Struct. Eng.*, 132(2), 244–252.

Shen, J., Kitjasateanphun, T., and Srivanich, W. (2000). "Seismic performance of steel moment frames with reduced beam sections." *Eng. Struct.*, 22(8), 968–983.

Shenton III, H. W., and Lin, A. N. (1993). "Relative performance of fixed-base and base-isolated concrete frames." *J. Struct. Eng.*, 119(10), 2952–2968.

Somerville, P., Anderson, D., Sun, J., Punyamurthula, S., and Smith, N. (1998). "Generation of ground motion time histories for performance-based seismic engineering." *Proc. 6th, U.S. National Conf. of Earthquake Engineering*, Earthquake Engineering Research Institute, Oakland, CA.

Taghavi, S., and Miranda, E. (2003). "Response assessment of nonstructural building elements." *PEER Rep. No. 2003–05*, Pacific Earthquake Engineering Research Center, Univ. of California, Berkeley, CA.

Tsai, K. C., and Popov, E. P. (1988). "Steel beam-column joints in seismic moment resisting frames." *Rep. No. UCB/EERC-88/19*, Earthquake Engineering Research Center (EERC), Univ. of California, Berkeley, CA.